RESEARCH

Magnetic micro-archaeology: a method for conducting rock magnetic microfacies analysis on archaeological soil micromorphology samples, with a case study from El Salt, Alcoy, Spain

Ada Dinçkal[1,2,3] · Angel Carrancho Alonso[4] · Cristo M. Hernandez Gomez[1] · Carolina Mallol[1,2]

Abstract

For geoarchaeologists the use of multiproxy and multimethod integrative approaches has become common for studying the sedimentary context of archaeological materials. In this paper, we introduce a novel approach that combines rock magnetic analysis with micromorphological analysis. We first conduct a brief examination of the magnetic properties of organic resins used in micromorphology to understand the potential impact of the resin and manufacturing process on the magnetic signature. It is crucial to understand the original production of the samples to ensure that endothermic reactions do not compromise the magnetic data. We illustrate the advantages of this approach through a case study of a pit hearth from the Neanderthal archaeological site of El Salt in Alcoi, Spain. This study utilises archived micromorphological samples of a pit hearth (combustion structure H77) initially described by Leierer et al. (J Archaeol Sci 123:105237, 2020). Rock magnetic analysis of multiple magnetic parameters—including magnetic susceptibility, natural remanent magnetization, and progressive isothermal remanent magnetization—reveals that each microfacies type exhibits a unique magnetic pattern, even if there is overlapping in signatures across some magnetic parameters. The interpretation of the magnetic data aligns with the results and microfacies descriptions previously provided by Leierer et al. (J Archaeol Sci 123:105237, 2020), further supporting the interpretation of the combustion feature as being in situ with a history of repeated use. The approach presented here offers an enhanced tool for micromorphologists to better understand the magnetic characteristics of microfacies units in higher resolution and establish direct connections to the micromorphological results.

Keywords Archaeomagnetism · Micromorphology · Microarchaeology · Geoarchaeology · Neanderthals · Archaeological sciences · Archaeological methodology

✉ Ada Dinçkal
adinckal@ull.edu.es

1 Área de Prehistoria, Arqueología E Historia Antigua, Departamento de Geografía E Historia, Facultad de Humanidades, Universidad de La Laguna, Campus de Guajara, 38071 La Laguna, Santa Cruz de Tenerife, Spain

2 Archaeological Micromorphology and Biomarkers (AMBI Lab), Instituto Universitario de Bio-Orgánica Antonio González (IUBO), Universidad de La Laguna, Apartado 456, 38206 La Laguna, Santa Cruz de Tenerife, Spain

3 Laboratorio de Paleomagnetismo, Dpto. Física, Escuela Politécnica Superior, Edificio A1, Universidad de Burgos, Avda. Cantabria S/N 09006, Burgos, Castile and León, Spain

4 Área de Prehistoria, Dpto. Historia, Geografía y Comunicación, Laboratorio de Prehistoria, Edificio I+D+I, Universidad de Burgos, Plaza Misael Bañuelos S/N. 09001, Burgos, Castile and León, Spain

Introduction and background

Geoarchaeology has expanded its scope in recent years, focusing on the holistic integration of analytical methods to achieve more profound interpretations. Presented here is a pilot study for directly integrating rock, or environmental, magnetic analysis with archaeological soil micromorphology. We highlight that rock magnetism and micromorphology can be performed on the same samples increasing the analytical resolution of the magnetic study. By integrating these methods, new interpretative potentials can be achieved, allowing rock magnetism to integrate more thoroughly with other geoarchaeological analyses. The study includes an analysis of the magnetic properties of organic resins to understand what magnetic alterations may occur during the production of micromorphological samples. This is followed by an opportunistic case study of a pit hearth from the

archaeological site of El Salt in Alcoi, Spain. We analysed the rock magnetic properties of archived micromorphological samples originally described by Leierer et al. (2020) to highlight the strengths of this approach.

Soil micromorphology is an important tool used by geoarchaeologists to examine the microscopic composition of archaeological soils and sediments—the primary context for archaeological material and an artefact in itself (Karkanas and Goldberg 2018, Goldberg and Berna 2010). Micromorphology is a robust tool for combining different types of analysis, including chemical and mineralogical analytical methods to reconstruct past human behaviour (see chapters in Nicosia and Stoops 2017; Wilson 2017; Mentzer 2017; Berna 2017). Since its inception in the 1970s (Goldberg 1979), micromorphology has become crucial in understanding the original geogenic, biogenic, or anthropogenic processes that form archaeological contexts (Karkanas and Goldberg 2018; Goldberg and Aldeias 2018), which can reveal otherwise invisible anthropogenic contexts such as bedding structures (Goldberg et al. 2009; Miller et al. 2013), manipulated soils (Karkanas et al. 2015), and anthropogenic processes forming combustion features (e.g., Mallol et al. 2013; Mallol and Henry 2017; Leierer et al. 2020; Karkanas 2021). Micromorphology is frequently integrated with other geoarchaeological methods such as Fourier transforms infrared spectroscopy (see Weiner et al. 1993, 2002; Karkanas et al. 2000; Miller et al. 2016), X-ray fluorescence, scanning electron microscopy, and X-ray diffraction (Berthold and Mentzer 2017; Mentzer 2017; Wilson 2017), as well as the study of archaeological biomarker (e.g., Mallol et al. 2013; Connolly et al. 2019; Leierer et al. 2019; Rodríguez De Vera et al. 2020) and ancient DNA analysis (Massilani et al. 2022). Integrated geoarchaeological analysis using micromorphology is often conducted on the same material or directly in association between samples (e.g., Mentzer 2017; Berna 2017; Miller et al. 2016). This reuse of the micromorphological material allows for a direct association between what is described in the thin section and what is interpreted from the data.

Magnetic analysis has two primary applications in archaeology. Firstly, the study of the Earth's magnetic field and its direction is commonly used for the dating of archaeological sites (e.g., Herries and Adams 2013; Dirks et al. 2017) and to understand diachrony within archaeological palimpsests (Carrancho et al. 2016a, b; Zeigen et al. 2019). Secondly, environmental or rock magnetism is a method which studies the magnetic characteristics of iron-bearing minerals identifying the processes which formed them (Evans and Heller 2003; Dearing et al. 1996; Dearing 1999), which can be utilised as proxies for interpreting the anthropogenic, geogenic, or biogenic actions behind those processes within the archaeological context (Carrancho et al.

2016a, b; Church et al. 2007; Herries and Latham 2009; Zeeden and Hambach 2021). In palaeolithic contexts, this technique explores human behaviour relating to combustion (Herries and Fisher 2010; Dinçkal et al. 2022). More recent rock magnetic studies in archaeology explore processes of site formation (Ozán et al. 2019; Bradák et al. 2020), with some studies noting a need for micromorphology to help interpret magnetic data (Bradák et al. 2020; Dinçkal et al. 2022). Although both micromorphology and rock magnetism explore the consequences of anthropogenic-driven processes, they operate at different scales. Therefore, while there are many examples of sites which utilise both methodologies, there are fewer examples of studies which use them in tandem (e.g., Kapper et al. 2014; Lowe et al. 2018; Ozán et al. 2019; Leierer et al. 2020; Reidsma et al. 2021). Even in these examples, studies lack deep integration between the methods and only achieve superficial corroboration in the final interpretations. This paper will provide a pilot study for how to approach this integration and highlight the interpretive potentials which can be achieved. El Salt, Alcoi, in Spain (Fig. 1), is a Neanderthal open-air site with deposits dating between 60.7 and 45.2 ka ago (Galván et al. 2014). The deposits consist of mostly well-stratified, horizontally deposited geogenic sands containing a high concentration of archaeological remains and dense combustion features organised in 13 lithostratigraphic units (Galván et al. 2014). The deposits at El Salt have been extensively studied: lithics and archaeo-stratigraphy (Machado et al. 2017; Pérez et al. 2020; Mayor et al. 2020, 2022), zooarchaeological and microfaunal analysis (e.g. Marin-Monfort et al. 2021; Fagoaga et al. 2019), and archaeobotany (Vidal-Matutano 2017; Vidal-Matutano et al. 2017, Vidal-Matutano et al. 2018). This has included a host of multi-method geoarchaeological research including micromorphology and archaeomagnetism exploring the combustion material on the site (Mallol et al. 2013; Leierer et al. 2019; Herrejón Lagunilla et al. 2019; Leierer et al. 2020), biomarkers exploring lipid components within the site (Mallol et al. 2013; Leierer et al. 2019, 2020; Sistiaga et al. 2014) and aDNA to understand the formation of the Neanderthal gut biome, which was identified for the first time through the integrated use of micromorphology and biomarker analysis (Rampelli et al. 2021). For this pilot study, we conducted rock magnetic analyses on micromorphological material previously studied by Leierer et al. (2020). Leierer et al. explored a potential pit hearth with the use of micromorphology in combination with lipid biomarkers, zooarchaeological assessment, burning experiments on substrata, and the use of archaeo- and rock magnetism. Our study focuses on the analysis of two archived micromorphological monoliths, aiming to understand what magnetic data we can draw from them and how this may help the interpretations of the pit hearth.
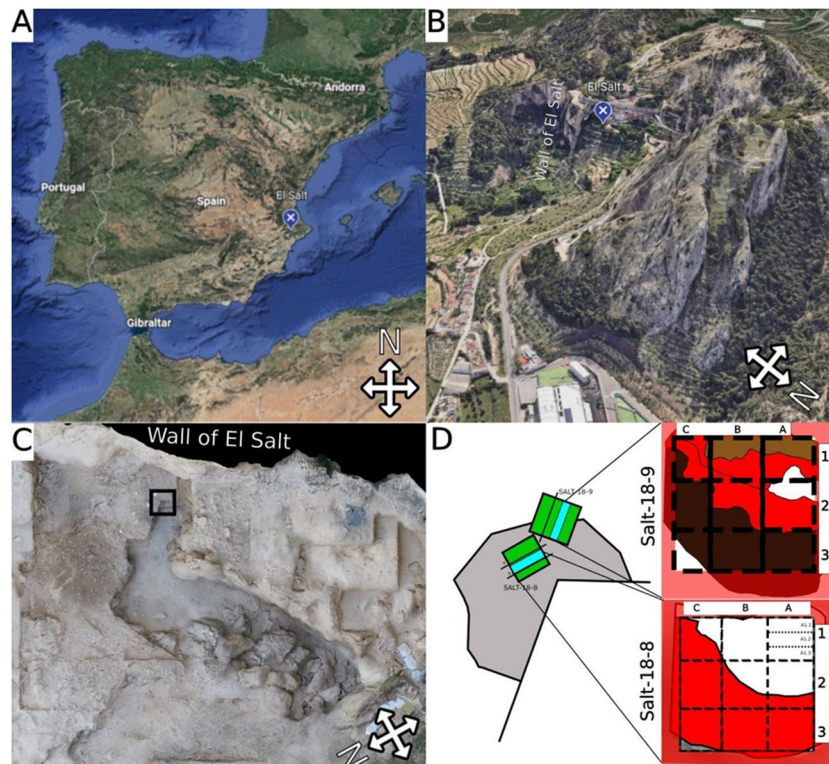
Fig. 1 **A** Location of El Salt in the Iberian Peninsula. Map taken from Google Earth. **B** Location of El Salt in the region around the city of Alcoi, 3D map from Google Earth showing the general landscape of the surrounding region. The Wall of El Salt refers to the overhanging cliff face which signifies the main wall of the rock shelter. **C** Orthophoto of the El Salt excavation area. Black box indicates the location of the pit hearth. **D** Schematic of the pit hearth and location of the micromorphological monoliths (green boxes). Black lines indicate location of thin sections in Leierer et al. (2020), while blue rectangles indicate location of micromorphological slabs subsampled for this study. Schematic of slabs shown to the right, White portions indicate White Layers (WL), Red portions indicate Red Layers (RL). Dark Brown portions refer to microfacies unit XI, and Light Brown zones refer to microfacies unit LSG11. Each of the slabs shows the divisions of their cubic samples, while cubic sample A1 for Salt-18–8 demonstrates an example of how microfacies samples were subdivided

Methods and material

The Pit Hearth—combustion structure H77

The Pit Hearth (combustion structure H77) is located at the base of lithological unit XB (see Fumanal García 1994; Galván et al. 2014), beginning between facies LSG14 and LSG11, and cuts into lithological unit XI. Leierer et al. (2020) interpret the combustion structure as in situ based on its well-stratified nature as well as the sharpness of the contact between the Red Layers (RL) and White Layers (WL). Micromorphological descriptions identify four microfacies units (MFUs) composing the pit hearth sequence (see Table 1). The lowest is 'XI', a dark brown unit composed of rich charcoal and other organic components with a microscopic brownish yellow groundmass (Fig. 1D, brown layer in Salt-18–9 schematic). Above is the Red Layer (RL) (Fig. 1D, Red units in micromorphological schematics), described as being similar to XI with a heavy reduction in organic material towards the hearth edge, in Salt-18–9, with almost no organic material at its centre (Salt-18–8). Experimental work conducted by Leierer et al. (2020) demonstrated that when microfacies type XI is burnt, it rubifies, indicating that RL is a thermally altered form of XI. The RL sharply transitions into the White Layer (WL) MFU, a dominant ash unit with some presence of faunal fragments and *Celtis australis* seed coats but little else. The WL once again transitions sharply, now into the MFU LSG11.

Archaeomagnetic analysis in Leierer et al. (2020) reveals a stable magnetic signature with a well-preserved directional record, something unlikely to occur if the hearth were an ash dump. Microscopic observations also show minimal evidence of rip-up clast and disturbance of the ash structures. There is evidence for repeated use of the combustion feature, primarily in the form of two ash lenses separated by an interloping RL, potentially an artefact of the pit wall structure crumbling, as well as the WL's thickness indicating multiple accumulations of ash (Leierer et al. 2020; Karkanas 2021). Fuel sources included wood and unknown plant fuel, with temperatures in the RL layers rising to around 500 and 600 °C.

Table 1 Description of microfacies units and the sampling of each unit for the analysis of magnetic properties

Microfacies unit	Location and microfacies sampling	Description (per Leierer et al. 2020)
LSGII	LSGI1, found exclusively in Salt-18–9, is represented by two microfacies samples and deposited above the White Layer from Stratigraphic Unit XB at El Salt	Coloured brown due to charcoal and black organic residues. Shares similar microstructure and anthropogenic components with XI, with a less decalcified matrix
White Layer	WL is present in both Salt-18–8 and Salt-18–9. WLs are represented by 14 samples, 13 from Salt-18–8 and a single sample from Salt-18–9. In both samples the WL is located above the RL. Contact between the overlying and underlying units is sharp	In thin section, WL is up to 5 cm thick. Microstructure is predominantly intergrain microaggregate and vughy with occasional channels. It is locally fibrous and composed exclusively of wood ash and unidentified plant ash. Few components besides ash are present, with bone fragments being the most abundant. (Microscope PPL) Appears pale-yellowish brown. (Microscope XPL) Is locally light grey, containing calcium carbonate pseudomorphs likely of wood ash rhombs, or blueish grey zones which lack rhombs and show scattered micritic crystals
Red layer	The red layer is represented by 27 samples in both Salt-18–8 ($n=16$) and Salt-18–9 ($n=11$). Contact between the RL and the layers above it is sharp. Contact with XI directly below it is diffused and gradient. The primary distinction between XI and RL is the lower density of organic material and the rubification of the sediment in RL	Depending on the position within the feature, the RL is thicker, more reddish, and less organic towards the centre. Towards the edges it is thinner, with less rubification and increased (but still very little) organic matter towards the periphery. In some areas, towards the centre of the combustion structure, RL exhibits horizontal planes closer to the WLs. Micro-structure and voids are like that of MFT XI. (Microscope- PPL) Exhibits a massive reddish-brown sediment devoid of organic material. (Microscope-XPL) The b-fabric resembles that of MFT XI
XI	XI is expressed only in sample Salt-18–9 by 12 samples. It is located below the combustion structure, with diffuse and gradient contact with the deposit above (RL)	Microstructures predominant intergrain with a complementary subangular blocky microstructures. Complex packing voids, channels, and chambers. Anthropogenic components: possible fat-derived char, charcoal, and bone are very abundant. (Microscope- PPL) A dark brown colour in PPL with a brownish yellow groundmass. The dark brown colour is due to charcoal and black organic residues. (Microscope-XPL) The b-fabric is only weakly crystallitic, indicating decalcification. The mineral grains are also affected by decalcification

Sample preparation

Organic micromorphological resin samples were prepared at the Archaeological Micromorphology and Biomarkers (AMBI) Laboratory. Two sets of samples were prepared for the analysis of the organic resin's magnetic parameters. One utilised epoxy and one utilised a polyester styrene mixture, with the addition of > 1% accelerant. The artificial acceleration of the hardening can take as little time as a couple of hours depending on the sample, through an endothermic reaction which can heat the samples, as high as ~ 200 °C depending on the size and surface area of the sample (Jongerius and Heintzberger 1975; see Fig. 2B). Artificial heating can enhance magnetic signatures and cause the neoformation of magnetic minerals in previously unheated archaeological material. Heating does not exceed ~ 60 °C without accelerant, but the process can take weeks for the polyester resin to solidify. Artifical heating is not present with epoxy impregnation or samples without accelerant, and heating is reduced the smaller a sample is, or with an increase in surface area.

Polyester styrene mixture was utilised for our control sediment samples. Volcanic beach sand from Las Caletillas (Tenerife, Spain) was utilised due to the iron-oxide concentration in volcanic sand, which would highlight any magnetic enhancements through the use of accelerant during production. Two sets of samples were organised. One was impregnated in a rectangular shape with 1 lt of resin, while a second set of samples were impregnated in a cubic shape with 3.5 l of resin. A set of unconsolidated loose samples were utilised as a control.

Archaeological samples from El Salt were taken from archived material utilised by Leierer et al. (2020). Sample preparation can be found there. Only Salt-18–8 and Salt-18–9 had enough material to be analysed (see Fig. 1D for locations of samples). Sample preparation for magnetic analysis was conducted at the University of Burgos' Palaeomagnetism Laboratory. All samples were cut into 10-cc-sized cubes utilising an aluminium (non-ferromagnetic) bladed saw. Archaeological samples were similarly divided into fifteen 10-cc cubic samples, and three 8-cc samples, with a final number of 18 samples (referred to as archaeological cubic samples from here, see Fig. 1 for sample locations). After initial magnetic measurements, each of the cubic samples was subdivided into a further three samples which targeted distinctive microfacies units; these are labelled as Microfacies (MF) samples throughout the paper. From the
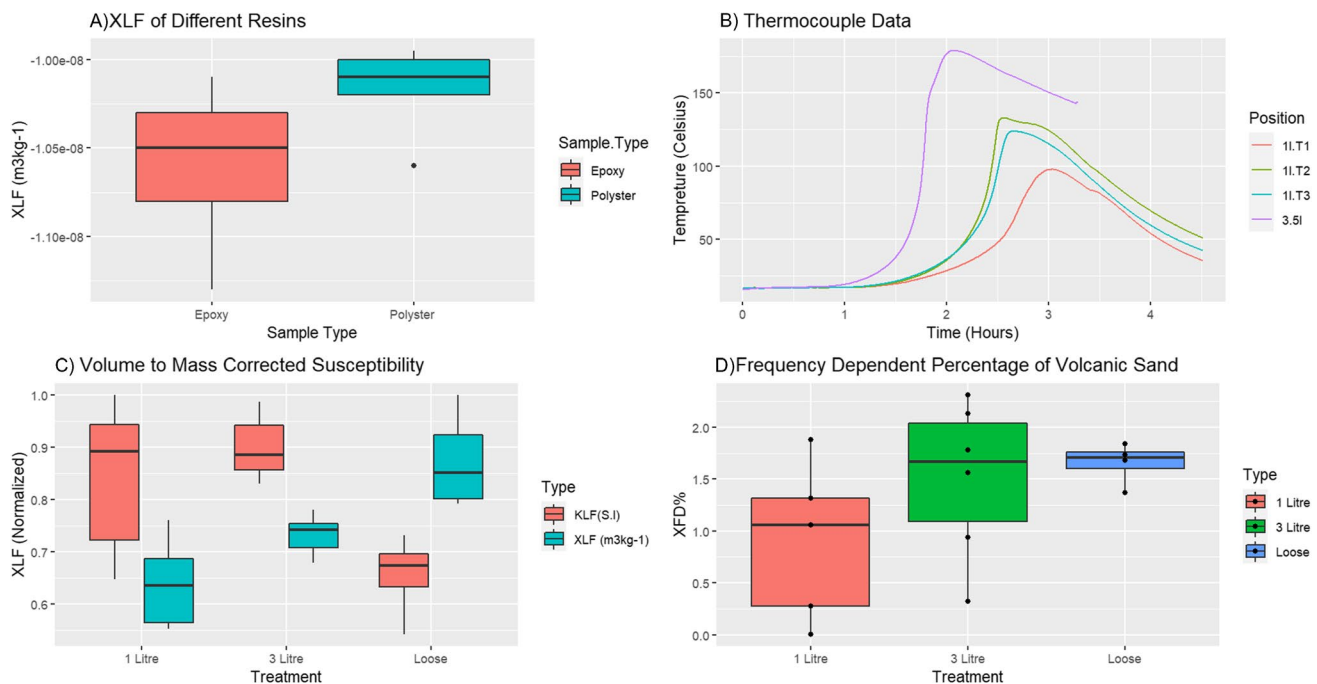
Fig. 2 Results for resin control analysis. **A** χ_{LF} for organic resins utilised in micromorphological samples. The results indicate very low or negative magnetic susceptibility indicating the resin is diamagnetic and unlikely to influence samples' own magnetism. **B** Thermocouple data for organic resins which have hardened with the use of accelerant. Three measurements taken from a sample with 1 l of resin utilised (red, green, and blue lines), and a single measurement taken from a 3-l sample (purple line). The maximum temperatures achieved were around 180 °C depending on the size of the sample and location. **C** Susceptibility values of volcanic sand impregnated with accelerant-induced resin demonstrating the influence of the potential chemical kinetic reactions. Red indicates volume susceptibility, and blue indicates mass correct susceptibility. Samples were normalised to the maximum value of each measurement type. **D** Frequency-dependent susceptibility percentages of volcanic sand results

Table 2 Description of magnetic results for microfacies units. The main mineralogical components between the various units appear to be mostly the same; they are composed of magnetite with varying compositions of Single-Domain and Superparamagnetic grains. This is visible within both the MF samples analysed as well as those in the balance. White Layers have an enhanced magnetic susceptibility (Fig. 4B), natural remanent magnetization (Fig. 4C), and SIRM (Fig. 5C, E) likely due to a higher concentration of ferrimagnetic minerals. RL shows some enhancement that is not as pronounced as the WL. Figure 7 shows that the most enhanced values for the RL are those near the WLs. Less enhanced expression of RL aligning with those of the XI and LSG11. RL layers also separated themselves with large XFD%, which are dominantly SP grains. Unit XI have MS and NRM values which are reflective of less enhanced RL values but have XFD% values which are like WLs

Microfacies unit	XLF (m^{3}kg^{-1})	NRM (Am^{2}kg^{-1})	IRM (A/m^2)	Hysteresis and Day plots (see S.I.)	Summary of magnetic mineralogy
LSGII	The two samples measured (S189A1.1 and S189B1.1) have XLF values of 1.19×10^{-6} (m^{3}kg^{-1}) and 1.39×10^{-6} (m^{3}kg^{-1}) respectively, with XFD% 11.9% and 10.3%. The XFD% is within the SP-dominated range	Sample S189A1.1 possesses an NRM value of 14×10^{-5} (Am^{2}kg^{-1}) and Qn values of 3.14. Sample S189B1.1 possesses an NRM value of 1.50×10^{-5} (Am^{2}kg^{-1}) and Qn values of 2.92	A sole LSG11 sample underwent IRM, displaying an SIRM value of 10×10^{-3} (A/m^2) and an S-Ratio of 1. A single balance sample was measured with an S-ratio of 0.99 (refer to S.I.). Indicating low-coercive minerals as a primary driver	Hysteresis loops reinforce that LSG11 is driven by magnetite. On a Day plot this samples plots within the 'PSD' zone	The few expressions of LSG11 fall within the range of SP dominance of ferrimagnetic (s.l) minerals
White Layer	XLF ranges from 2.580×10^{-6} (m^{3}kg^{-1}) to 5.970×10^{-6} (m^{3}kg^{-1}) with a mean of 3.429×10^{-06}. XFD% range from 2.4%, single domain dominant, to 11.8%, SP dominant. The mean values sit around 8.1% which is a mixture of SD and SP grains, with an increased influence of SP particles	NRM values range from 5×10^{-5} (Am^{2}kg^{-1}) through 85×10^{-5} (Am^{2}kg^{-1}) with a mean 3×10^{-5} (Am^{2}kg^{-1}). Qn ratios range from 0.55 through 5.7 with a mean of 3	11 samples were measured for IRM. SIRM values ranged from 14.1300×10^{-3} (A/m^2) through 33.79×10^{-3} (A/m^2). S-ratio ranges from 0.96 through 1, with a mean 0.99. 5 associated balance samples had S-ratios varying from 0.99 through 1. S-ratio indicates a strong dominance of Low-Coercive minerals. However, few samples show a minor increased presence of high-coercive minerals demonstrating some heterogeneity within the samples	Hysteresis loops of all WL samples show a dominance of low-coercive minerals which are likely magnetite (as per Leierer et al. 2020); furthermore, they all plot within the PSD region of the Day Plots	White Layers have the highest values and highest mean values of χ_{LF}, NRM, and SIRM indicating that this MFU is the most magnetically enhanced. WL are driven by a high concentration of magnetite grains with a large variability of domain structures ranging from dominantly single-domain (<7%) through the dominantly superparamagnetic (10%>). On average these values fall towards an SP influenced domain structure. Qn ratios show clear evidence of thermal alteration, with values distinctively above unity. Only a single sample falls below this, which may be due to the presence of bone within the substrate

Table 2 (continued)

Microfacies unit	XLF (m^3kg^{-1})	NRM (Am^2kg^{-1})	IRM (A/m^2)	Hysteresis and Day plots (see S.I.)	Summary of magnetic mineralogy
Red layer	XLF values vary from 7.48×10^{-6} (m^3kg^{-1}) through 21.30×10^{-6} (m^3kg^{-1}) with a mean of 1.34×10^{-6} (m^3kg^{-1}). XFD% values vary from 7.2%, indicating a mixture of SD with an increasing influence of SP grains, to a max above 14% (14% being the maximum achievable percentage difference), demonstrating dominant SP concentrations	NRM values range from 3.60×10^{-5} (Am^2kg^{-1}) through 29.00×10^{-5} (Am^2kg^{-1}) with a mean 13×10^{-5} (Am^2kg^{-1}). Qn ratios range from 0.98 through 6.56 with a mean of 2.62	Four RL MF samples underwent IRM. SIRM values: 7.01×10^{-3} (A/m^2), 11.98×10^{-3} (A/m^2), 8.76×10^{-3} (A/m^2), and 3×10^{-3} (A/m^2), with corresponding S-ratios: 0.99, 0.93, 0.97, and 0.96, signifying a strong prevalence of low-coercivity minerals like magnetite. However, the S-ratio results also reveal a slight increase in high-coercivity minerals compared to other microfacies units (MFUs). Nine additional RL samples were analysed with the balance. S-ratios range from 0.98 to 1. The data exhibit a notable pattern: samples from the Hearth's center (Salt-18–8) predominantly possess an S-ratio of 1, except for sample S188B3.3 located at the bottom. Conversely, samples from the Hearth's edge (Salt-18–9) exhibit S-ratios of either 0.98 or 0.99. This pattern is reflected in the IRM. The single sample from the hearth's centre has the lowest S-ratio (0.99) compared to those from edge	Hysteresis loops show a dominance of low-coercive minerals, identified as magnetite in Leierer et al. (2020), with Day plotting in the PSD region	Red Layers are composed of primarily magnetite with domain sizes that range from superparamagnetic with some SD influence, to completely SP dominated. IRM analysis indicates that there is some influence of high-coercive minerals, such as hematite. This presence of high-coercive minerals is primarily present along the outer edges of the hearth. It has been previously noted that SP hematite particles will influence magnetic remanence less; thus. the increase of SP hematite within the layers may explain the rubification of the red layers in the centre but the reduced expression in the S-ratio and IRM (Butler 1973)
XI	XLF values range from 0.42×10^{-6} ($m^{3*}kg^{-1}$) to 1.31×10^{-6} (m^3kg^{-1}). XFD% values range from 2.7%, primarily SD driven, through 12.3%, primarily SP driven, with a mean of 8.5% indicating a mixture of SD and SP grains with an increase in SP	NRM values range from 2.10×10^{-5} (Am^2kg^{-1}) to 15.00×10^{-5} Am^2kg^{-1}) with a mean of 6.98×10^{-5} (Am^2kg^{-1}). Qn values range from 1.113 through 3.172 with a mean of 1.93	2 samples from XI were measured with IRM, while 3 were measured with the balance. SIRM are 7×10^{-3} (A/m^2) and 9.23×10^{-3} (A/m^2), and S-ratio for all 5 measurements are either 0.99 or 1 indicating a very strong presence of low-coercive minerals	Like the other MFUs, hysteresis loops show a low coercive mineral component with Day plotting in the region PSD region. However, XI tends to plot on its own away from the other MFUs	XI layers are driven by magnetite primarily composed of domain sizes also varying from SD dominant to SP dominant. Generally, XI layers appear to have less magnetic enhancement than RL layers, and distinctively less enhancement than WLs

A) Magnetic Susceptibility

C) Frequency Dependent Perentage (%)

B) Natural Remenant Magnetisation (NRM)

D) Qn Ratios
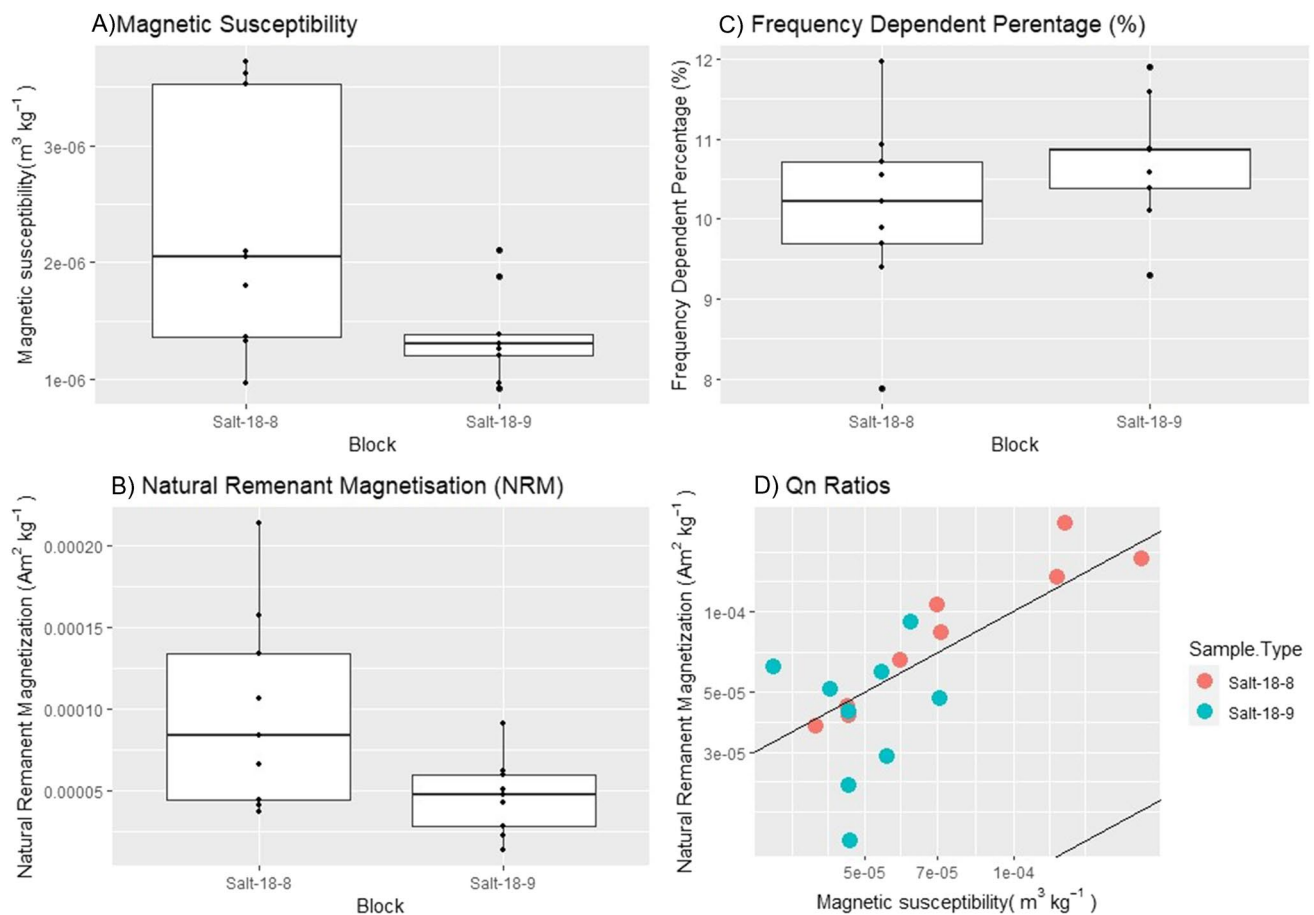
Fig. 3 Results for cubic samples. **A** χ_{LF} values. SALT-18–8 has a mean value of 2.71×10^{-6} (m³kg⁻¹). SALT-18–9 has a mean of 1.38×10^{-6} (m³kg⁻¹). The difference in χ_{LF} can be explained as Salt-18–8 is taken from the centre of the pit hearth structure and has a larger concentration of ash compared to Salt-18–9. **B** Natural Remenant Magnetization values; susceptibility patterns are repeated in the NRM. Salt-18–8 has a mean of 9.80×10^{-5} (Am²kg⁻¹), once again higher than Salt-18–9, with a mean of 4.669×10^{-5} (Am²kg⁻¹).

C $\chi_{FD\%}$. all but a single sample is 9% > indicating that the driver of magnetic susceptibility is superparamagnetic particles. **D** Qn ratios for cubic samples. Salt-18–8 are consistently with a mean of 1.139. Salt-18–9 has a mean of 0.99. Salt-18–9 has supposedly less combusted units explaining why values are lower. However, samples with the highest Qn ratios are S189B3 and S189C3, which are composed of theoretically not combusted unit XI (see Fig. 1)

same set of cubes, 18 additional samples were subsampled to be measured with a Variable Field Translation Balance; these are referred to as balance samples in this paper.

Magnetic analysis

Magnetic susceptibility is the ease a material can be magnetised; it is often dictated by the concentration and type of ferromagnetic (*s.l.*) minerals as well as their granulometry (Dearing 1999; Tauxe 2010). Measurements were conducted utilising both a KLY-4 Kappabridge (AGICO, noise level 3×10^{-8} S.I.), denoted in this paper as MS, and a Bartington MS2 Dual Frequency susceptibility metre, denoted in this paper as χ_{LF} for mass corrected values and κ_{LF} for volume susceptibility. Dual Frequency Magnetic Susceptibility (χ_{FD}) can identify ferrimagnetic minerals in the range of

Multi-domain (MD), Single-Domain (SD), and Superparamagnetic (SP) domain sizes by comparing the magnetic susceptibility attained at a high (χ_{HF} or κ_{HF}) and low-frequency (χ_{LF} or κ_{LF}) magnetic field (Dearing 1999). Finer domain structures contribute less to the magnetic signature at higher frequency magnetic fields, and the percentage difference between the two measurements can identify compositional concentrations of different domains (Dearing et al. 1996).

Natural Remenant Magnetization (NRM) was measured for archaeological samples with a 2G SQUID magnetometer (noise level 5×10^{-12} Am²). NRM refers to the magnetization a sample retained outside of an applied field (Evans and Heller 2003). Sixteen MF samples were selected for progressive acquisition of Isothermal Remenant Magnetization (IRM) analysis utilising a Magnetic Measurements MMPM10 5 T pulse magnetizer along with the 2G SQUID magnetometer. Progressive IRM

slowly magnetises a sample with a steadily increasing magnetic field until the sample's magnetization reaches saturation. Different compositions of ferrimagnetic minerals saturate at different fields, with low coercivity minerals, such as magnetite or maghemite, saturating before 300 miliTesla (mT), while high-coercivity minerals, such as hematite and goethite, saturate at above ~ 1000 mT. All samples were magnetised until 2000 mT.

Eighteen microfacies samples were analysed utilising the Variable Field Translation Balance (MM_VFTB) to calculate further progressive isothermal remanent magnetization (IRM) curves, as well as hysteresis loops (± 1 T) and back-field coercivity curves. These parameters reflected the compositional magnetic mineralogical assemblage with hysteresis loops providing further information that can be utilised in understanding grain size and domains of ferrimagnetic minerals (Tauxe et al. 1996, 2002). High temperature thermomagnetic experiments (e.g., magnetization or susceptibility curves) were not carried out because the samples were resin impregnated. However, ferromagnetic composition is known for these samples from Leierer et al. (2020).

Statistical analysis of the data was conducted using R Studios (Team, R. C. 2021) and the ggPlot2 package (Wickham 2016). Balance data was analysed utilising the RockMag Analyzer program (Leonhardt 2006).

Results and discussion

Results: resin control analysis

Measurements of organic resins show weak magnetic susceptibility values ranging from -0.0113×10^{-6} (m^{3}kg^{-1}) to -0.009×10^{-6} (m^{3}kg^{-1}) (see Fig. 2A), indicating the predominance of diamagnetic minerals. Therefore, this should not alter the overall magnetic signature of samples with a prevalence of ferromagnetic (*s.l.*) minerals (like H77), essentially replacing the influence of air.

Temperatures reached during accelerant-induced hardening of resin exceeded 150 °C (Fig. 2B). Figure 2C highlights an issue that may occur when comparing consolidated samples with unconsolidated samples. The diamagnetic resin is insignificant in altering the magnetic signature of our samples, replacing the influence of air. However, resin is heavier than air. When mass corrections are applied to the κ_{LF} values, the added weight of the resin artificially dilutes the magnetic signature. Blue boxes in Fig. 2C show the mass corrected susceptibility (χ_{LF}), where we find that the loose bulk samples appear more enhanced than the impregnated samples. As the impregnated samples have been heated to between 150 and 200 °C, it is expected that they would be more enhanced, not less. In κ_{LF} (Fig. 2C, red boxes), this pattern is completely reversed. It is important to note that this impregnation itself should not change the quantity of

magnetic minerals within the volumetric space—if anything, it is the heat that may generate a magnetic enhancement—or alter the fabric of the sedimentary unit, as this would defeat the purpose of micromorphological analysis. Therefore, the primary explanation is an artificial dilution of the magnetic signature caused by the greater weight of the resin (compared to air). This artificial dilution does not affect the patterns in the magnetic parameter; thus, it does not alter the analysis conducted on the samples. It only makes it difficult to compare impregnated samples to non-impregnated material with mass-corrected measurements. Direct analysis of data between the two sets of samples in different mediums should be conducted with volumetric magnetic susceptibility assuming the volumes of the samples are the same.

The values of magnetic susceptibility per volume of the volcanic sand samples (Fig. 2C, values in red) show a clear enhancement of the magnetic signature occurring within the samples consolidated with resin, as those in the resin are significantly more enhanced than loose samples. However, this does not seem to have occurred with the samples' domain structures, where all the samples sit at ~ 2% χ_{FD} margin (Fig. 2D). The heat reached through accelerant use does enhance the magnetic signature, but the proportion of superparamagnetic (SP) minerals does not change completely. This highlights the importance of understanding if the samples were annealed utilising accelerating agents, leading to endothermic effects during production. Samples influenced by accelerants will have altered magnetic signatures and are not suitable for study.

Archaeological samples

Tables 1 and 2 present descriptions of the microfacies units and their magnetic properties. Figure 3 presents the magnetic parameters of cubic samples, while Figs. 4 and 5 present magnetic parameters for MF units and associated IRM results respectively. All the microfacies have baseline similar magnetic parameters. They are composed of magnetite with varying compositions of Single-Domain and Superparamagnetic grains. This is visible within both the MF samples analysed as well as those in the balance. Corrected hysteresis loops possess pot-bellied morphologies and plot within the Pseudo Single Domain (PSD) region of Day plots (Day et al. 1977, Dunlop 2002). The Day plot PSD region is not entirely informative of the PSD dominance of the grains, and many samples can plot in that region for reasons such as the heavy admixture of SD/SP-grained minerals (Tauxe et al. 1996, 2002). This admixture of SD/SP domain grains is further reinforced by the $\chi_{FD\%}$, which shows mean values for all of the MFU between 8 and 11%.

We can broadly compare the magnetic susceptibility and NRM results with those published by Leierer et al. (2020); direct comparison of results is not possible as the data is

A) Distribution of Magnetic Susceptibiity to Domain Str
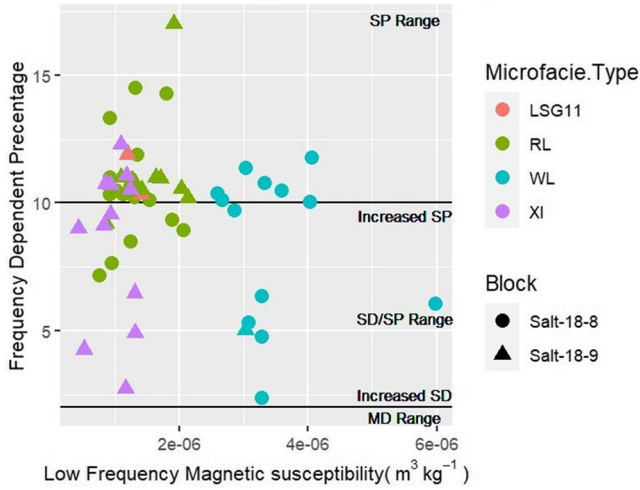
B) Magnetic Susceptibility by Microfacies
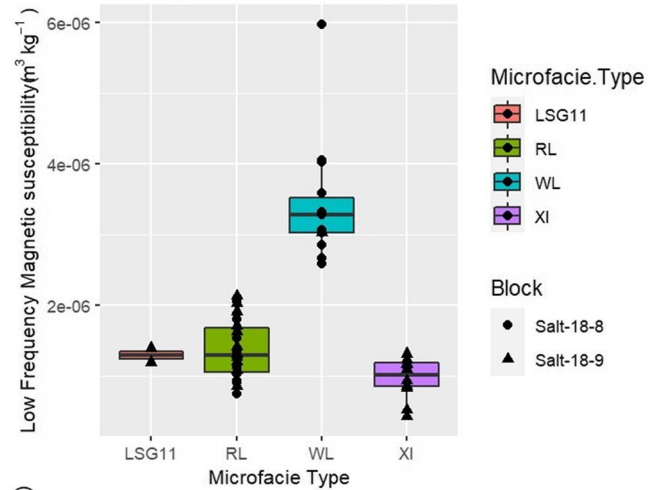
C) NRM by Microfacies
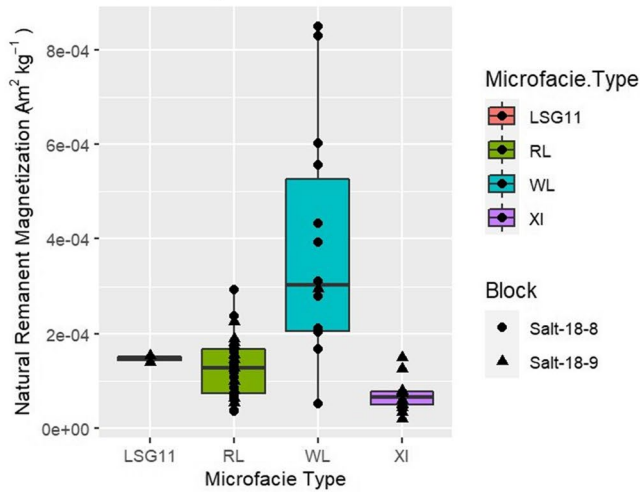
D) Frequency Dependent MS by Microfacies
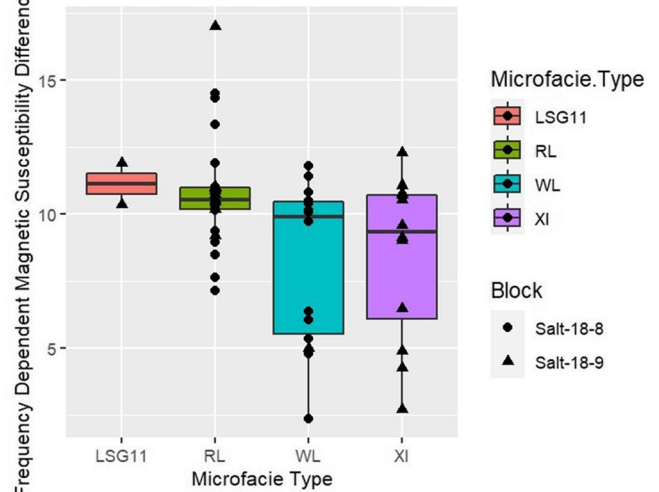
E) Qn ratios
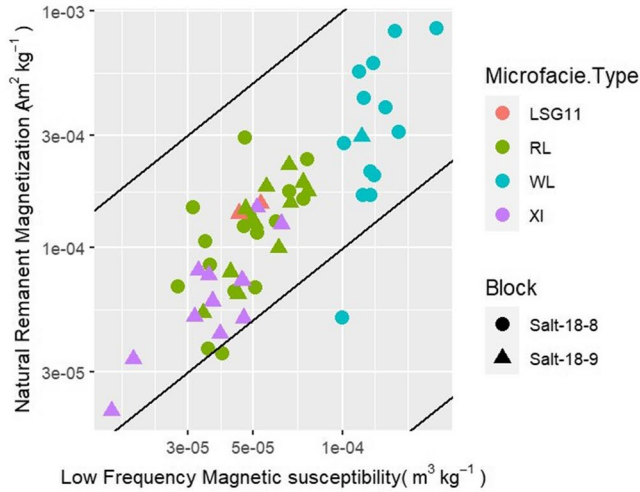
F) Day Plot
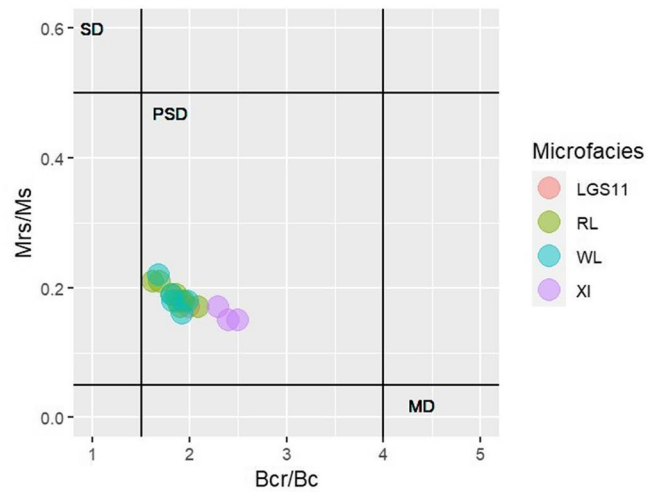
◀**Fig. 4** Results for microfacies samples. **A** χ_{LF} (x-axis) and $\chi_{FD\%}$ (y-axis) plotted against one another with indication on the primarily identified domain ranges. Distribution of **B** χ_{LF}, **C** NRM values, and **D** $\chi_{FD\%}$ separated by microfacies. WL has the strongest enhancement of magnetic susceptibilities and remanence but also contains a wide range of $\chi_{FD\%}$ domains. **E** Qn ratios separated by microfacies, both X and Y axis are on a logarithmic scale. **F**. Day plots are separated by microfacies. The primary differentiating factor is MS and NRM, which is particularly visible in plot (**E**) highlighting the Qn ratios. All but two samples are above unity. These two samples are samples S188A1.2B, Qn = 0.54, and S188C3.2, Qn = 0.97, which are a WL and an RL respectively. All other measurements have Qn ratios above unity, indicating that there is some level of thermal alteration to all microfacies units

derived from samples consolidated in different mediums. However, the overall patterning is complimentary. Leierer et al. (2020) present results which indicate that the WL layers are significantly more enhanced in their magnetic susceptibility and NRM than the RL. This differentiation is also in the intensity of the remanent magnetization, with the WL having significantly higher SIRM than the strongest RL samples.

The Konigsberger (*Qn*) ratio (*cf.* Stacey 1967), [NRM/χH], being χ the magnetic susceptibility by H the local Earth's magnetic field, provides an understanding of the thermal stability of the sample set. Ratios above unity (*Qn* = 1) are generally assumed to carry a thermal remanent magnetization (TRM) or a partial TRM (pTRM) (Stacey 1967; Carrancho et al. 2009). Leierer et al. (2020) published *Qn* results obtained in standard (~10 cc) cubic specimens which were centred at unity (*Qn* = 1) with only a single specimen falling below that value. In our case, while there is more variability within the cubic samples' *Qn* ratios, the measurements taken from the centre of the hearth (Salt-18–8) follow this same pattern (Fig. 3D). Measurements taken from the edge of the hearth (Salt-18–9) have distinctively more variability with some samples being well below unity while others being above. When we compare the cubic samples to the MF samples, we find that the overall values of the MF *Qn* ratios increase (Figs. 4E and 6; Table 3). Figure 6 demonstrates that MF samples (mean *Qn* = 2.58) have higher *Qn* ratio values than those of the cubic samples (mean *Qn* = 1.05). Table 3 highlights the stark elevation of *Qn* ratios from individual cubic samples compared to their MF subsamples, which occur when a single sample is reduced to its microfacies units. There is a single exception to this pattern—S188A1, which is composed completely of WL (see Table 3). MF subsamples A1.1 and A1.3 follow the standard pattern of *Qn* ratios (at least twice that of A1 cube). However, MF sample A1.2B has a *Qn* ratio of 0.55, less than half of A1 (*Qn* ratio = 1.23). Similarly, A1.2 MF sample, which is taken from the same location as A1.2B, does not show strong increase either (*Qn* = 1.42). Sample S188A1.2B is anomalous as it is from the WL, thus thermally altered.

The sample contains the lowest values of MS and NRM of WL, with $\chi_{FD\%}$ above 10%, indicating the lower concentration of ferrimagnetic minerals, which are dominantly SP. SP grains do not contribute to magnetic remanence (which would lower NRM values; Butler 1973), but does contribute to susceptibility. This may cause the *Qn* ratio to tend towards lower values. Leierer et al. (2020) note minimal evidence for bioturbation affecting this unit. Therefore, it is unlikely that the severe reduction of *Qn* ratio is driven by the intrusion of unburnt material into the deposit or noticeable disorder affecting the remanent record.

Cubic samples with the lowest *Qn* ratios are typically found at the edges of the hearth (Salt-18–9; Fig. 3D), which is not unexpected given the likely increase of uncombusted material towards these areas. However, an interesting anomaly is observed in some areas where the micromorphological analysis identifies combustion materials, but *Qn* ratio values are lower than those from supposedly unheated specimens. All the samples with *Qn* ratios lower than unity (e.g., S189A2, S189B1, and S189B2) contain multiple distinctive microfacies units (as shown in Fig. 7 and Table 3), containing any combination of RLs, WLs, and XI. In contrast, samples that are uniform but supposedly uncombusted, e.g., microfacies XI (Sample S189A3 and S189B3), exhibit higher *Qn* ratios. The reduced *Qn* ratios may result from different magnetic behaviours across multiple stratigraphic units conflicting with each other. As highlighted by samples S189A2 and S189B1, which have the lowest *Qn* ratios for the cubic samples, values increase significantly when subdivided into individual MF units. This increase in the *Qn* ratio is most prominent in combusted microfacies units, while samples which are supposedly uncombusted, MFU XI, show minimal enhancement in microfacies samples. It is interesting to note that the highest level of enhancement experienced from cubic to microfacies samples is those from the centre of the hearth (Salt-18–8). Except for the previously discussed Salt188A1.2B, all microfacies samples measured here are distinctively more enhanced. Cubic samples are mostly uniform in WL or RLs with no obvious microstratigraphy outside of the microfacies units. It is possible that the increase in *Qn* ratios within these units is not reflective of conflicting magnetic behaviours of multiple microfacies units, but conflicting magnetic behaviour of multiple microstratigraphic depositions within a single microfacies unit. In this situation, the significant increase of *Qn* ratios from cubic to the microfacies samples could be evidence for multiple micro stratigraphic depositions.

The presence of multiple microstratigraphic domains could be stronger evidence for multiple depositions, particularly in the ash layers. Ash layers have been previously shown to heavily deflate over time, with thicker ash sequences being representations of either repeated
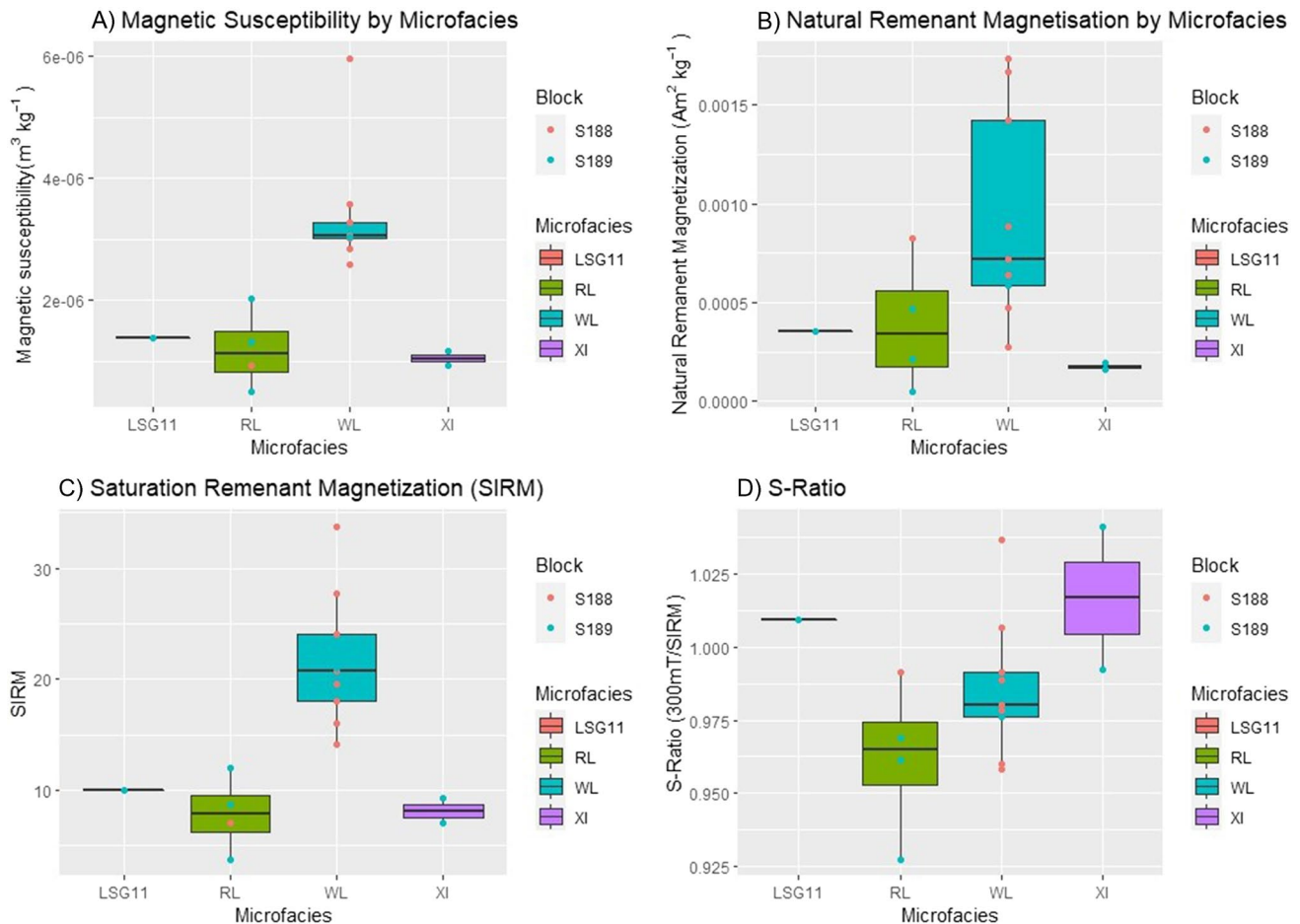
Fig. 5 All measured magnetic parameters for samples measured with IRM analysis. **A** χ_{LF}, **B** NRM, **C** SIRM, **D** S-ratios. Samples are dominantly low-coercive minerals (e.g., magnetite). All non-RL units have a mean S-ratio of 0.99 or 1 indicating almost complete dominance of low coercive minerals. RL have a mean S-ratio of 0.96, indicating a slight increase in high-coercive mineral concentration. Sample with lower S-ratios are from the edges of the hearth. This is minimised but reflected in balance measured S-ratios which range from 0.98 through unity (see S.I). The small increase in high-coercive minerals is important to the identification of the RL, which is rubified, a process occurring when hematite is formed through combustion (Canti and Linford 2000; Mentzer 2014). Despite the distinctive red colour, the 'hematite' concentration in these measurements appears low. Higher $\chi_{FD\%}$ likely contributes to this as SP particles do not express within remanence, i.e., NRMs or IRM measurements (Butler 1973). If the high-coercive component is primarily SP, then the overall expression in the S-ratio will be minimised. This minimization is especially highlighted at the centre of the hearth, where RL is at its most rubified but S-ratio shows no high-coercive minerals

burnings or a single very extensive burning (Karkanas 2021). However, a single extensive burning is more likely to create a singular homogenous magnetic signature and may not contain this pattern of microstratigraphic domains—unless churned up by factors of bioturbation. Leierer et al. (2020) indicate little evidence for bioturbation disturbing the hearth's microstructure and does indicate some evidence for repeated burnings in the form of multiple ash layers and red soil being found present between those ash lenses. This anomaly within the *Qn* ratios may further reinforce this interpretation. However, further experiments are needed to investigate this anomalous behaviour. Furthermore, the increase in *Qn* ratios across all microfacies units indicates that whether affected

by the H77 combustion feature directly or not, there is some thermal influence on the magnetic signature of all microfacies explored in this study, even those XI units which are thermally unaltered.

While the variation between microfacies is easy to note, the level of heterogeneity within samples should also be highlighted. Figure 7 shows the location of the primary magnetic properties analysis for all samples within the two slabs. Leierer et al. (2020) pointed out the general trend that magnetic values decreased with depth in the combustion structure and this trend is primarily reflected in the difference between the microfacies, as the WL layers being strong than those of RL layers in both χ_{LF} and NRM (Fig. 7B, D). XI and the RL have

Fig. 6 Comparing Koeningsberger (Qn) ratios for cubic, circles, samples and MF, triangles, samples
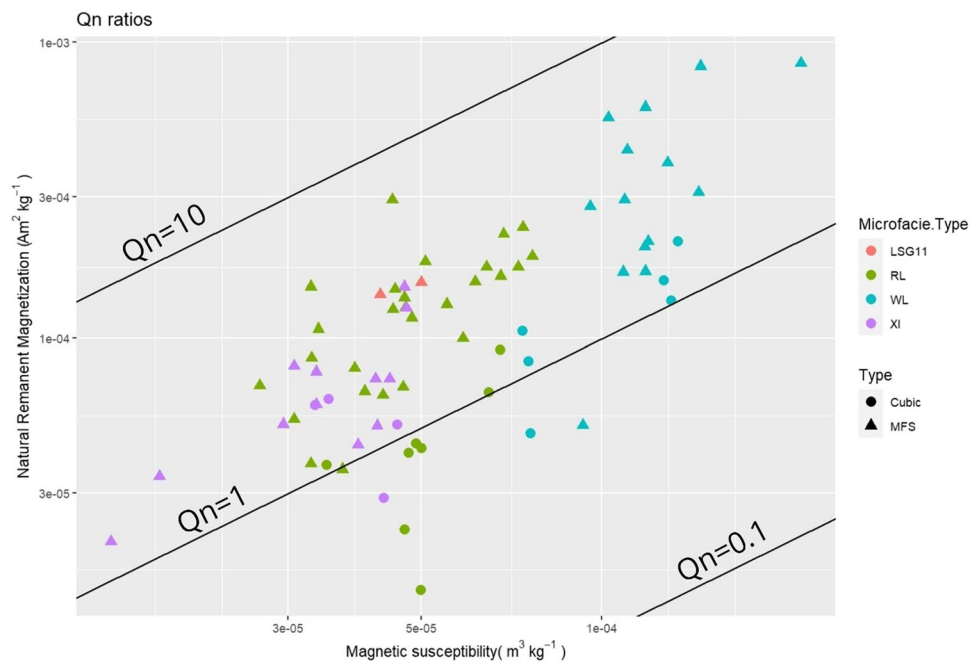
a large amount of overlap in both their χ_{LF} and NRM (Fig. 7B, D). This overlap occurs in the lower range of RL values, and their maximum χ_{LF} and NRM values are higher than those from XI (see Fig. 4). However, we find that the RL NRM measurements physically closer to WL MFs tend to have stronger values. There is still a fair amount of heterogeneity within the distribution of the values. Leierer et al. (2020) described the difference between the two deposits being due to the presence of a large organic component within the XI and then in the RL layers. Organic material, which would primarily be diamagnetic in magnetic signature, would likely act as a diluting component to the XI magnetic signature, along with the thermal magnetic enhancement altering the RL closer to the combustion area would thus define the variation in the magnetic signatures between these two layers.

In the WL layers this heterogeneity is not reflected in the $\chi_{LF,}$ which is uniformly high, but is visible in both the $\chi_{FD\%}$ (Fig. 7C) and the Qn ratios (Fig. 7E). The $\chi_{FD\%}$ for WL varies from 2.5% through > 14%. It is interesting to note that, when comparing the NRM to the $\chi_{FD\%}$ we find that the sample with the lower $\chi_{LF\%}$ in the hearth's centre (Salt-18–8 A1.2, A1.3, A2.1, B2.2) tends to correspond to greater NRM expression. This trend is less pronounced in more peripheral samples (Salt 18–8, C1.1, and Salt 18–9 A2.1), which exhibit lower $\chi_{FD\%}$ and more moderate NRM values. An explanation for the reduced $\chi_{FD\%}$ in combusted layers could be in the mechanical removal of superparamagnetic particles. Leierer et al. (2020) note that layers XI and RL have the largest evidence for decalcification.

Decalcification occurs within soil primarily due to the movement of slightly lower pH water through the deposit. Such a process is also often noted to remove finer magnetic mineral and SP domain particles from deposits (Herries 2006). Despite this, the RLs have the highest $\chi_{FD\%}$ of any microfacies unit (Fig. 7C). This could have multiple explanations. Decalcification somehow occurred during the burning process, or just before the formation of the finer SP domain magnetic minerals. Conversely, finer SP particles were introduced after the burning, and after the decalcification. A cause of this could be found in the translocation of SP minerals from the WL ash component, which is expected to have a higher $\chi_{FD\%}$ compared to the RL due to its exposure to more burning (Herries and Fisher 2010; Dinçkal et al. 2022). The original deposition of ash has extremely low mass density with extreme porosity, more than 85% of the volume being air, after initial combustion (Karkanas 2021). During the formation of the overlying deposit, strong compression could move finer particles through this highly porous deposit into the RLs. This could be further helped with some movement of water through the WLs. Although the WL layer has little evidence for decalcification, there is evidence for recalcification indicating some moisture movement (Leierer et al. 2020). A further explanation is the action of repeated burnings has been noted as a likely depositional mechanic in this pit hearth. Furthermore, as a combustion feature is exposed to more burnings, the $\chi_{FD}\%$ increases due to an increased SP grain concentration (Herries and Fisher 2010). The increase in RL $\chi_{FD}\%$ compared to the WL occurs despite the WLs being exposed to more frequent burning events. However, it has also been noted that

Table 3 Qn values of cubic samples compared to their MF subsamples

Salt -18–8						Salt-18–9					
Sample	Primary MF	Qn	Sample	MF	Qn	Sample	Primary MF	Qn	Sample	MF	Qn
A1	WL	1.23	A1.1	WL	2.14	A1	RL	1.35	A1.1	LSG11	3.27
			A1.2	WL	1.42						
			A1.2B	WL	0.55				A1.2	RL	2.40
			A1.3	WL	3.96				A1.3	RL	2.52
A2	WL	1.44	A2.1	WL	3.92	A2	WL	0.63	A2.1	WL	2.70
			A2.2	WL	1.77						
			A2.2B	WL	1.54				A2.2	RL	2.47
			A2.3	RL	6.56				A2.3	RL	1.73
A3	RL	0.86	A3.1	RL	2.78	A3	XI	1.13			
			A3.2	RL	3.19				A3.1	XI	1.74
			A3.2B	RL	4.56				A3.2	XI	1.78
			A3.3	RL	2.56				A3.3	XI	1.74
B1	WL	1.59	B1.1	WL	5.69	B1	RL	0.85	B1.1	LSG11	3.09
			B1.2	WL	5.44				B1.2	RL	3.57
			B1.3	WL	2.91				B1.3	RL	3.28
B2	WL	1.11	B2.1	WL	3.05	B2	RL	0.28	B2.1	RL	2.70
			B2.2	WL	5.11				B2.2	RL	2.05
			B2.3	RL	2.71				B2.3	XI	1.85
B3	RL	0.90	B3.1	RL	2.42	B3	XI	1.79	B3.1	XI	2.30
			B3.2	RL	1.64				B3.2	XI	2.62
			B3.3	RL	1.15				B3.3	XI	3.17
C1	WL	1.03	C1.1	WL	1.72	C1	RL	0.48	C1.1	RL	1.70
			C1.2	RL	1.47				C1.2	RL	1.49
			C1.3	RL	3.21				C1.3	RL	3.24
C2	RL	1.02	C2.1	RL	2.37	C2	XI	0.67	C2.1	XI	1.64
			C2.2	RL	2.39				C2.2	XI	1.11
			C2.3	RL	2.93				C2.3	XI	1.20
C3	RL	1.07	C3.1	RL	2.60	C3	XI	1.79	C3.1	XI	2.68
			C3.2	RL	0.98				C3.2	XI	1.35

after a set number of burnings, the $\chi_{FD\%}$ decreases to around 8%, potentially due to the aggregation of finer magnetic minerals acting like SD particles (Carrancho et al. 2009; Herries and Fisher 2010; Dinçkal et al. 2022). This pattern is reflected within the study here, as the $\chi_{FD}\%$ of WL layers are distinctively lower than those of the RL layers, sitting around a mean of 8.1%. Repeated burnings would impact RL less due to increasing insulation by the WL, preventing a reduction in the $\chi_{FD\%}$.

The results achieved by this opportunistic analysis of the El Salt pit hearth complement those published by Leierer et al. (2020), while also further reinforcing interpretations of the pit hearth. Here, the magnetic results seem to further indicate that there is a consistent deposition and relighting of the combustion structure over a sustained period. Furthermore, the anomalies of the *Qn* ratios seem to further reinforce that the hearth was not formed by a sustained long-term combustion event but by repeated reuse of the hearth itself.

Viability of methodology and future application

In this paper, we demonstrated the feasibility of conducting some detailed rock magnetic analysis on samples impregnated by micromorphological resins. There are two major constraints to such analysis. If an accelerant is used during sample manufacture, it will cause samples to heat thus altering magnetic properties. Conversely, due to the resin's toxicity when combusted, thermal rock magnetic analysis cannot be conducted. Research design should take these two constraints into account when applying. Our study was opportunistic, utilising archived material, and thus sampling was not designed around our application. Future research considering this approach from the onset will likely achieve more robust interpretations of the results.

Directly being able to analyse micromorphological material integrates rock magnetic analysis with micro-contextual geoarchaeological analysis. Contextualising
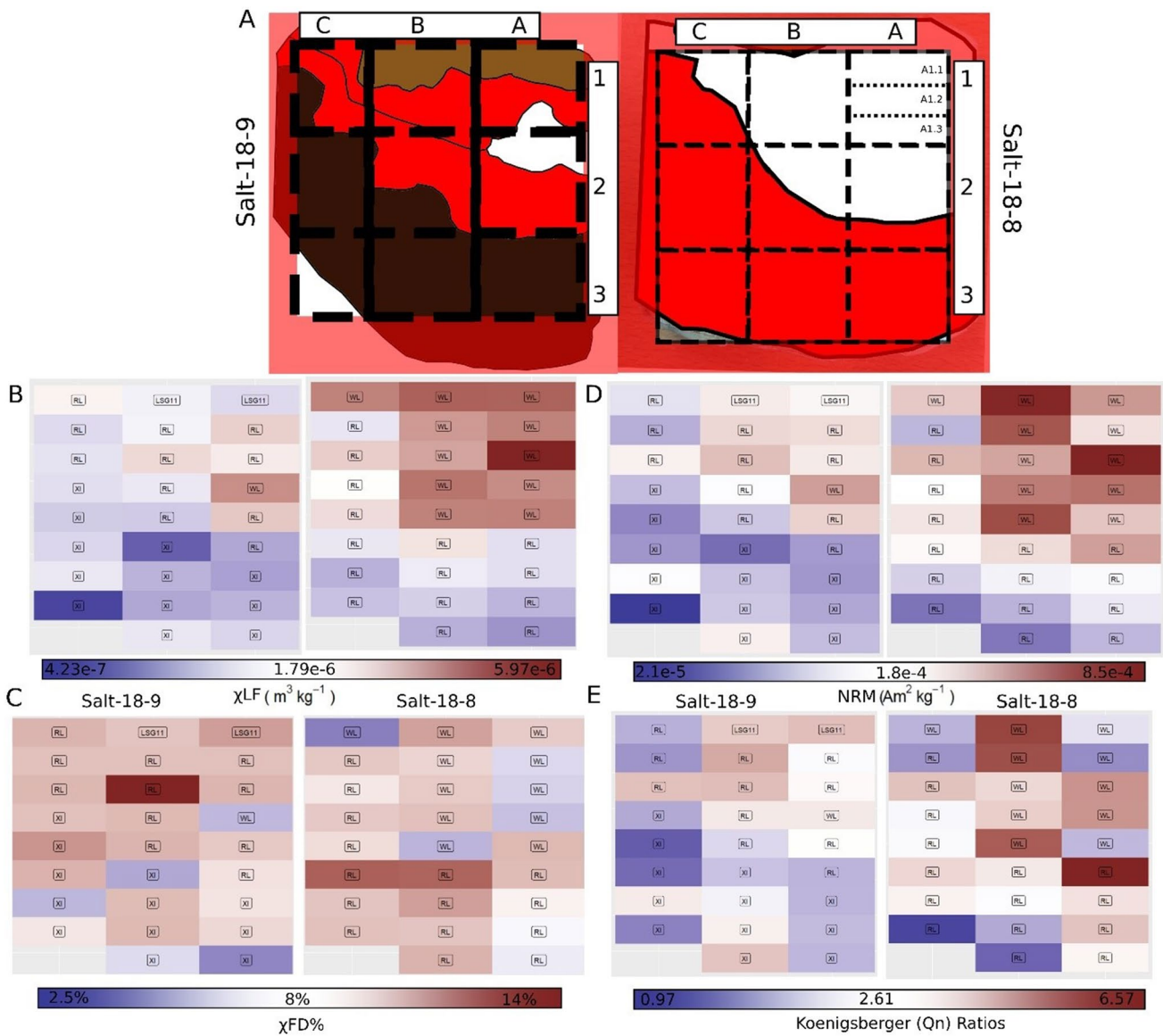
Fig. 7 Distribution of magnetic parameters. **A** Position of cubic samples (colours as in Fig. 1), sample A1 for Salt-18–8 provides a graphical representation of how all cubic samples were subdivided into MF samples. **B** Location of MS samples, **C** location of XFD% values. **D** Location of NRM values and **E** location of Qn ratios. Note, samples S188A1.2B, S188A2.2B, and S188A3.2B are not represented within these figures as they correlate to the same position as associated sample numbers

magnetic results this way increases the resolution in which the archaeological magnetic data can be analysed and interpreted. For example, our study highlighted enhanced *Qn* ratio on finer individual microfacies sample data which may be a product of relighting or multiple-combustion-driven depositions. However, rock magnetic reference work is lacking for the magnetism of microfacies units 'in situ'. Further experimental work is required to interpret these patterns. This approach provides the opportunity to look at archived micromorphological material for new

magnetic analysis, allowing for new data without resampling a site. However, this is only possible if the original recipe for the samples manufacture is recorded.

While the results presented here are promising, this is simply an opportunistic pilot study. Utilising micromorphology as a connective tissue between different methods, further research can and should focus on integrating this magnetic analysis more thoroughly with other geo-archaeological methods of mineralogical, chemical, and elemental analysis.

Conclusions

Within this paper, we have analysed the magnetic influence of sedimentary samples impregnated with organic resins, finding that the resin is diamagnetic, and should not influence the magnetic behaviour of sedimentary samples, as long as an accelerant is not used in the samples manufacture. We have conducted a further analysis of archived micromorphology samples at the neanderthal site of El Salt, Alcoi, that explored the in situ magnetic properties of separate microfacies units as presented by Leierer et al. (2020). This provides an increased level of resolution to the interpretation of magnetic data, while directly integrating it with micromorphological interpretations. The rock magnetic data indicates that while different microfacies have overlapping magnetic properties the sum of their magnetic behaviour was unique. Furthermore, enhancements in the *Qn* ratios between cubic and microfacies samples seem to emphasise the likelihood of multiple depositions, which further reinforced the interpretation of multiple combustion events from micromorphological results. Overall, we have found that the addition of rock magnetic analysis directly upon micromorphological samples provides a new approach to geoarchaeology analysis, providing meaningful data at higher resolutions for the interpretation of combustion features. Future work should look at connecting this method with other geoarchaeological methods as well as developing experimental work exploring the magnetic behaviour of microfacies units.

Declarations

References

Berna F (2017) FTIR microscopy. In: Nicosia C, Stoops G (eds) Archaeological soil and sediment micromorphology. John Wiley & Sons, Ltd., pp 411–415. https://doi.org/10.1002/9781118941065.ch39

Berthold C, Mentzer SM (2017) X-ray Microdiffraction. In: Nicosia N, Stoops G (eds) Archaeological soil and sediment micromorphology. John Wiley & Sons, Ltd., pp 417–429. https://doi.org/10.1002/9781118941065.ch40

Bradák B, Carrancho Á, Herrejón Lagunilla Á, Villalaín JJ, Monnier GF, Tostevin G, Mallol C, Pajović G, Baković M, Borovinić N (2020) Magnetic fabric and archaeomagnetic analyses of anthropogenic ash horizons in a cave sediment succession (Crvena Stijena site, Montenegro). Geophys J Int 224(2):795–812. https://doi.org/10.1093/gji/ggaa461

Butler RF (1973) Stable single-domain to superparamagnetic transition during low-temperature oxidation of oceanic basalts. J Geophys Res(1896-1977) 78(29):6868–6876. https://doi.org/10.1029/JB078i029p06868

Canti MG, Linford N (2000) The effects of fire on archaeological soils and sediments: temperature and colour relationships. Proc Prehist Soc 66:385–395. https://doi.org/10.1017/S0079497X00001869

Carrancho Á, Villalaín JJ, Angelucci DE, Dekkers MJ, Vallverdú J, Vergès JM (2009) Rock-magnetic analyses as a tool to investigate archaeological fired sediments: a case study of Mirador cave (Sierra de Atapuerca, Spain). Geophys J Int 179(1):79–96. https://doi.org/10.1111/j.1365-246X.2009.04276.x

Carrancho Á, Herrejón Lagunilla Á, Vergès JM (2016a) Three archaeomagnetic applications of archaeological interest to the study of burnt anthropogenic cave sediments. Quatern Int 414:244–257. https://doi.org/10.1016/j.quaint.2015.10.010

Carrancho Á, Villalaín JJ, Vallverdú J, Carbonell E (2016b) Is it possible to identify temporal differences among combustion features in Middle Palaeolithic palimpsests? The archaeomagnetic evidence: a case study from level O at the Abric Romaní rock-shelter (Capellades, Spain). Quatern Int 417:39–50. https://doi.org/10.1016/j.quaint.2015.12.083

Church MJ, Peters C, Batt CM (2007) Sourcing fire ash on archaeological sites in the Western and Northern Isles of Scotland, using

mineral magnetism. Geoarchaeology 22(7):747–774. https://doi.org/10.1002/gea.20185

Connolly R, Jambrina-Enríquez M, Herrera-Herrera AV, Vidal-Matutano P, Fagoaga A, Marquina-Blasco R, Marin-Monfort MD, Ruiz-Sánchez FJ, Laplana C, Bailon S, Pérez L, Leierer L, Hernández CM, Galván B, Mallol C (2019) A multiproxy record of palaeoenvironmental conditions at the Middle Palaeolithic site of Abric del Pastor (Eastern Iberia). Quatern Sci Rev 225:106023. https://doi.org/10.1016/j.quascirev.2019.106023

Day R, Fuller M, Schmidt VA (1977) Hysteresis properties of titanomagnetites: grain-size and compositional dependence. Phys Earth Planet Inter 13(4):260–267. https://doi.org/10.1016/0031-9201(77)90108-X

Dearing JA (1999) Magnetic susceptibility. In: Walden J, Oldfield F, Smith JP (eds) Environmental magnetism: a practical guide, vol 6. Quaternary Research Association, pp 25–62

Dearing JA, Dann RJL, Hay K, Lees JA, Loveland PJ, Maher BA, O'Grady K (1996) Frequency-dependent susceptibility measurements of environmental materials. Geophys J Int 124(1):228–240. https://doi.org/10.1111/j.1365-246X.1996.tb06366.x

Dinçkal A, Fisher EC, Herries AIR, Marean CW (2022) Mapping magnetism: geophysical modelling of stratigraphic features by using in situ magnetic susceptibility measurements at Pinnacle Point 5-6 North, South Africa. Geoarchaeology (37):840–857. https://doi.org/10.1002/gea.21924

Dirks PH, Roberts EM, Hilbert-Wolf H, Kramers JD, Hawks J, Dosseto A, Duval M, Elliott M, Evans M, Grün R, Hellstrom J, Herries AI, Joannes-Boyau R, Makhubela TV, Placzek CJ, Robbins J, Spandler C, Wiersma J, Woodhead J, Berger LR (2017) The age of Homo naledi and associated sediments in the Rising Star Cave, South Africa. eLife 6:e24231. https://doi.org/10.7554/elife.24231

Dunlop DJ (2002) Theory and application of the Day plot (Mrs/Ms versus Hcr/Hc) 1. Theoretical curves and tests using titanomagnetite data. J Geophys Res: Solid Earth 107(B3):EPM 4–1-EPM 4–22. https://doi.org/10.1029/2001JB000486

Evans M, Heller F (2003) Environmental magnetism: principles and applications of enviromagnetics, vol 86. Academic Press

Fagoaga A, Laplana C, Marquina-Blasco R, Machado J, Marin-Monfort MD, Crespo VD, Hernández CM, Mallol C, Galván B, Ruiz-Sánchez FJ (2019) Palaeoecological context for the extinction of the Neanderthals: a small mammal study of Stratigraphic Unit V of the El Salt site, Alcoi, eastern Spain. Palaeogeogr Palaeoclimatol Palaeoecol 530:163–175. https://doi.org/10.1016/j.palaeo.2019.05.007

Fumanal García MP (1994) El yacimiento musteriense de El Salt (Alcoi, País Valenciano). Rasgos geomorfológicos y climatoestratigrafía de sus registros. SAGVNTVM, 39–55

Galván B, Hernández CM, Mallol C, Mercier N, Sistiaga A, Soler V (2014) New evidence of early Neanderthal disappearance in the Iberian Peninsula. J Hum Evol 75:16–27. https://doi.org/10.1016/j.jhevol.2014.06.002

Goldberg P (1979) Micromorphology of sediments from Hayonim Cave. Israel CATENA 6(2):167–181. https://doi.org/10.1016/0341-8162(79)90006-7

Goldberg P, Aldeias V (2018) Why does (archaeological) micromorphology have such little traction in (geo)archaeology? Archaeol Anthropol Sci 10(2):269–278. https://doi.org/10.1007/s12520-016-0353-9

Goldberg P, Berna F (2010) Micromorphology and context. Quatern Int 214(1–2):56–62. https://doi.org/10.1016/j.quaint.2009.10.023

Goldberg P, Miller CE, Schiegl S, Ligouis B, Berna F, Conard NJ, Wadley L (2009) Bedding, hearths, and site maintenance in the Middle Stone Age of Sibudu Cave, KwaZulu-Natal South Africa. Archaeol Anthropol Sci 1(2):95–122. https://doi.org/10.1007/s12520-009-0008-1

Herrejón Lagunilla Á, Carrancho Á, Villalaín JJ, Mallol C, Hernández CM (2019) An experimental approach to the preservation potential of magnetic signatures in anthropogenic fires. PLoS ONE 14(8):e0221592. https://doi.org/10.1371/journal.pone.0221592

Herries AIR (2006) Archaeomagnetic evidence for climate change at Sibudu Cave. South Afr Humanit 18(1):131–147

Herries AIR, Adams JW (2013) Clarifying the context, dating and age range of the Gondolin hominins and Paranthropus in South Africa. J Hum Evol 65(5):676–681. https://doi.org/10.1016/j.jhevol.2013.06.007

Herries AIR, Fisher EC (2010) Multidimensional GIS modeling of magnetic mineralogy as a proxy for fire use and spatial patterning: evidence from the Middle Stone Age bearing sea cave of Pinnacle Point 13B (Western Cape, South Africa). J Hum Evol 59(3–4):306–320. https://doi.org/10.1016/j.jhevol.2010.07.012

Herries AIR, Latham AG (2009) Archaeomagnetic studies at the Cave of Hearths. In: McNabb J, Sinclai AGM (eds) The cave of hearths: Makapan' Middle Pleistocene research project, vol. 1. Archaeopress, pp 59–64. https://doi.org/10.30861/9781407304205

Jongerius A, Heintzberger G (1975) Methods in soil micromorphology. A technique for the preparation of a large thin section, vol. 10. Netherlands Soil Survey Institue

Kapper KL, Anesin D, Donadini F, Angelucci DE, Cavulli F, Pedrotti A, Hirt AM (2014) Linking site formation processes to magnetic properties. Rock- and archeomagnetic analysis of the combustion levels at Riparo Gaban (Italy). J Archaeol Sci 41:836–855. https://doi.org/10.1016/j.jas.2013.10.015

Karkanas P (2021) All about wood ash: long term fire experiments reveal unknown aspects of the formation and preservation of ash with critical implications on the emergence and use of fire in the past. J Archaeol Sci 135:105476. https://doi.org/10.1016/j.jas.2021.105476

Karkanas P, Bar-Yosef O, Goldberg P, Weiner S (2000) Diagenesis in prehistoric caves: the use of minerals that form in situ to assess the completeness of the archaeological record. J Archaeol Sci 27(10):915–929. https://doi.org/10.1006/jasc.1999.0506

Karkanas P, Brown KS, Fisher EC, Jacobs Z, Marean CW (2015) Interpreting human behavior from depositional rates and combustion features through the study of sedimentary microfacies at site Pinnacle Point 5–6, South Africa. J Hum Evol 85:1–21. https://doi.org/10.1016/j.jhevol.2015.04.006

Karkanas P, Goldberg P (2018) Reconstructing archaeological sites: understanding the geoarchaeological matrix. John Wiley & Sons. https://doi.org/10.1002/9781119016427

Leierer L, Jambrina-Enríquez M, Herrera-Herrera AV, Connolly R, Hernández CM, Galván B, Mallol C (2019) Insights into the timing, intensity and natural setting of Neanderthal occupation from the geoarchaeological study of combustion structures: a micromorphological and biomarker investigation of El Salt, unit Xb, Alcoy Spain. Plos One 14(4):e0214955. https://doi.org/10.1371/journal.pone.0214955

Leierer L, Carrancho Alonso Á, Pérez L, Herrejón Lagunilla Á, Herrera-Herrera AV, Connolly R, Jambrina-Enríquez M, Hernández Gómez CM, Galván B, Mallol C (2020) It's getting hot in here—microcontextual study of a potential pit hearth at the Middle Paleolithic site of El Salt Spain. J Archaeol Sci 123:105237. https://doi.org/10.1016/j.jas.2020.105237

Leonhardt R (2006) Analyzing rock magnetic measurements: the RockMagAnalyzer 1.0 software. Comput Geosci 32:1420–1431. https://doi.org/10.1016/j.cageo.2006.01.006

Lowe KM, Mentzer SM, Wallis LA, Shulmeister J (2018) A multiproxy study of anthropogenic sedimentation and human occupation of Gledswood Shelter 1: exploring an interior sandstone rockshelter in Northern Australia. Archaeol Anthropol Sci 10(2):279–304. https://doi.org/10.1007/s12520-016-0354-8

Machado J, Molina FJ, Hernández CM, Tarriño A, Galván B (2017) Using lithic assemblage formation to approach Middle Palaeolithic settlement dynamics: El Salt Stratigraphic Unit X (Alicante, Spain). Archaeol Anthropol Sci 9(8):1715–1743. https://doi.org/10.1007/s12520-016-0318-z

Mallol C, Henry A (2017) Ethnoarchaeology of Paleolithic fire. Curr Anthropol 58(S16):S217–S229. https://doi.org/10.1086/691422

Mallol C, Hernández CM, Cabanes D, Sistiaga A, Machado J, Rodríguez Á, Pérez L, Galván B (2013) The black layer of Middle Palaeolithic combustion structures. Interpretation and archaeostratigraphic implications. J Archaeol Sci 40(5):2515–2537. https://doi.org/10.1016/j.jas.2012.09.017

Marin-Monfort MD, Fagoaga A, García-Morato S, Ruíz Sánchez FJ, Mallol C, Hernández C, Galván B, Fernández-Jalvo Y (2021) Contribution of small mammal taphonomy to the last Neanderthal occupations at the El Salt site (Alcoi, southeastern Spain). Quatern Res 103:208–224. https://doi.org/10.1017/qua.2021.4

Massilani D, Morley MW, Mentzer SM, Aldeias V, Vernot B, Miller C, Stahlschmidt M, Kozlikin MB, Shunkov MV, Derevianko AP, Conard NJ, Wurz S, Henshilwood CS, Vasquez J, Essel E, Nagel S, Richter J, Nickel B, Roberts RG, ... Meyer M (2022) Microstratigraphic preservation of ancient faunal and hominin DNA in Pleistocene cave sediments. Proc Natl Acad Sci 119(1):e2113666118. https://doi.org/10.1073/pnas.2113666118

Mayor A, Sossa-Ríos S, Molina FJ, Pérez L, Galván B, Mallol C, Hernández CM (2022) An instance of Neanderthal mobility dynamics: a lithological approach to the flint assemblage from stratigraphic unit viii of El Salt rockshelter (Alcoi, eastern Iberia). J Archaeol Sci Rep 44:103544. https://doi.org/10.1016/j.jasrep.2022.103544

Mayor A, Hernández CM, Machado J, Mallol C, Galván B (2020) On identifying Palaeolithic single occupation episodes: archaeostratigraphic and technological approaches to the Neanderthal lithic record of stratigraphic unit xa of El Salt (Alcoi, eastern Iberia). Archaeol Anthropol Sci 12(4). https://doi.org/10.1007/s12520-020-01022-4

Mentzer SM (2014) Microarchaeological approaches to the identification and interpretation of combustion features in prehistoric archaeological sites. J Archaeol Method Theory 21(3):616–668. https://doi.org/10.1007/s10816-012-9163-2

Mentzer SM (2017) Micro XRF. In: Nicosia C, Stoops G (eds) Archaeological soil and sediment micromorphology. John Wiley & Sons, Ltd., pp 431–440. https://doi.org/10.1002/9781118941065.ch41

Miller CE, Goldberg P, Berna F (2013) Geoarchaeological investigations at Diepkloof Rock Shelter, Western Cape, South Africa. J Archaeol Sci 40(9):3432–3452. https://doi.org/10.1016/j.jas.2013.02.014

Miller CE, Mentzer SM, Berthold C, Leach P, Ligouis B, Tribolo C, Parkington J, Porraz G (2016) Site-formation processes at Elands Bay Cave South Africa. South Afr Humanit 29(1):69–128

Nicosia C, Stoops G (eds) (2017) Archaeological soil and sediment micromorphology. John Wiley & Sons, Ltd. https://doi.org/10.1002/9781118941065

Ozán IL, Méndez C, Oriolo S, Orgeira MJ, Tripaldi A, Vásquez CA (2019) Depositional and post-depositional processes in human-modified cave contexts of west-central Patagonia (Southernmost South America). Palaeogeogr Palaeoclimatol Palaeoecol 532. https://doi.org/10.1016/j.palaeo.2019.109268

Pérez L, Machado J, Sanchis A, Hernández CM, Mallol C, Galván B (2020) A high temporal resolution zooarchaeological approach to Neanderthal subsistence strategies on the southeastern Iberian Peninsula: El Salt Stratigraphic Unit Xa (Alicante, Spain). In: Short-term occupations in Paleolithic archaeology. Springer International Publishing, pp 237–289. https://doi.org/10.1007/978-3-030-27403-0_10

Rampelli S, Turroni S, Mallol C, Hernandez C, Galván B, Sistiaga A, Biagi E, Astolfi A, Brigidi P, Benazzi S, Lewis CM, Warinner C, Hofman CA, Schnorr SL, Candela M (2021) Components of a Neanderthal gut microbiome recovered from fecal sediments from El Salt. Commun Biol 4(1). https://doi.org/10.1038/s42003-021-01689-y

Reidsma FH, Sifogeorgaki I, Dinçkal A, Huisman H, SierMJ, Van Os B, Dusseldorp GL (2021) Making the invisible stratigraphy visible: a grid-based, multi-proxy geoarchaeological study of Umhlatuzana Rockshelter, South Africa. Front Earth Sci 9. https://doi.org/10.3389/feart.2021.664105

Rodríguez De Vera C, Herrera-Herrera AV, Jambrina-Enríquez M, Sossa-Ríos S, González-Urquijo J, Lazuen T, Vanlandeghem M, Alix C, Monnier G, Pajović G, Tostevin G, Mallol C (2020) Micro-contextual identification of archaeological lipid biomarkers using resin-impregnated sediment slabs. Sci Rep 10(1). https://doi.org/10.1038/s41598-020-77257-x

Sistiaga A, Mallol C, Galván B, Summons RE (2014) The Neanderthal meal: a new perspective using faecal biomarkers. PLoS ONE 9(6):e101045. https://doi.org/10.1371/journal.pone.0101045

Stacey FD (1967) The Koenigsberger ratio and the nature of thermoremanence in igneous rocks. Earth Plant Sci Lett 2:67–68. https://doi.org/10.1016/0012-821x(67)90174-4

Stoops G (2021) Guidelines for analysis and description of soil and regolith thin sections, vol 184. John Wiley & Sons Ltd. https://doi.org/10.1002/9780891189763

Tauxe L, Mullender TAT, Pick T (1996) Potbellies, wasp-waists, and superparamagnetism in magnetic hysteresis. Journal of Geophysical Research: Solid Earth 101(B1):571–583. https://doi.org/10.1029/95JB03041

Tauxe L, Bertram HN, Seberino C (2002) Physical interpretation of hysteresis loops: micromagnetic modeling of fine particle magnetite. Geochem Geophys Geosyst 3(10):1–22. https://doi.org/10.1029/2001gc000241

Tauxe L (2010) Essentials of rock and paleomagnetism. University of California Press. https://doi.org/10.1525/9780520946378

Team RC (2021) R: a language and environment for statistical computing. https://www.R-project.org/

Vidal-Matutano P (2017) Firewood and hearths: Middle Palaeolithic woody taxa distribution from El Salt, stratigraphic unit Xb (Eastern Iberia). Quatern Int 457:74–84. https://doi.org/10.1016/j.quaint.2016.07.040

Vidal-Matutano P, Henry A, Théry-Parisot I (2017) Dead wood gathering among Neanderthal groups: charcoal evidence from Abric del Pastor and El Salt (Eastern Iberia). J Archaeol Sci 80:109–121. https://doi.org/10.1016/j.jas.2017.03.001

Vidal-Matutano P, Pérez-Jordà G, Hernández CM, Galván B (2018) Macrobotanical evidence (wood charcoal and seeds) from the Middle Palaeolithic site of El Salt, Eastern Iberia: palaeoenvironmental data and plant resources catchment areas. J Archaeol Sci Rep 19:454–464. https://doi.org/10.1016/j.jasrep.2018.03.032

Weiner S, Goldberg P, Bar-Yosef O (1993) Bone preservation in Kebara Cave, Israel using on-site Fourier transform infrared spectrometry. J Archaeol Sci 20(6):613–627. https://doi.org/10.1006/jasc.1993.1037

Weiner S, Goldberg P, Bar-Yosef O (2002) Three-dimensional distribution of minerals in the sediments of Hayonim Cave, Israel: diagenetic processes and archaeological implications. J Archaeol Sci 29(11):1289–1308. https://doi.org/10.1006/jasc.2001.0790

Wickham, H. (2016). ggplot2: elegant graphics for data analysis. Springer-Verlag, New York. https://ggplot2.tidyverse.org

Wilson CA (2017) Electron probe X-ray microanalysis (SEM-EPMA) techniques. In: Nicosia C, Stoops G (eds) Archaeological soil and sediment micromorphology. John Wiley & Sons, Ltd., pp 451–459. https://doi.org/10.1002/9781118941065.ch43

Zeeden C, Hambach U (2021) Magnetic susceptibility properties of loess from the Willendorf archaeological site: implications for the syn/post-depositional interpretation of magnetic fabric. Front Earth Sci 8. https://doi.org/10.3389/feart.2020.599491

Zeigen C, Shaar R, Ebert Y, Hovers E (2019) Archaeomagnetism of burnt cherts and hearths from Middle Palaeolithic Amud Cave, Israel: tools for reconstructing site formation processes and occupation history. J Archaeol Sci 107:71–86. https://doi.org/10.1016/j.jas.2019.05.001